CHAPTER 5

Volcanic Mound Fields and Lava Flow Fields on the East Pacific Rise, 16º-19ºS: Low Effusion Rate Eruptions at Overlapping Spreading Centers for the Last One Million Years

Abstract. Volcanic mound fields identified on SeaMARC II and HMR1 12 kHz side-scan data from the southern East Pacific Rise (SEPR) occur near overlapping spreading centers (OSCs) and migration traces of OSCs. The volcanic mound fields appear as a distinctive hummocky seafloor fabric caused by side-scan backscatter reflections from clusters of mound-shaped reflectors near the lower limit of system resolution. The lack of growth of the mound fields away from the ridge axis, and their occurrence in association with OSC traces, suggests that mound fields do not commonly evolve into off-axis volcanoes, but instead form along the ridge crest near OSCs. Volcanic mound fields coincide with the areas where pillow mounds are most abundant in high-resolution DSL-120 sonar. Since pillow mounds are constructed by low effusion rate eruptions, the volcanic mound fields found near the OSCs and in their migration traces suggest that volcanic effusion rates tend to be lower near ridge discontinuities than mid-segment regions. This tendency for low effusion rate eruptions at OSCs is documented for the past ~1 Myr. Three independent measurements of ridge segmentation, (1.) volcanic segment boundaries, marked by the low effusion rate eruptions, (2.) tectonic segments defined by OSCs, and (3.) magmatic segment boundaries based on continuity of parental magma composition , all coincide in the study area. The entire length of the ridge appears highly reflective on 12 kHz side-scan records, and we interpret this axial reflective zone (ARZ) as the zone about the ridge axis where all lava flows are sufficiently recent to be sediment-free to the penetration depth of 12 kHz sonar (10-50 cm). The ARZ width suggests extensive re-paving of the seafloor by lava flows typically occurs within 3-4 km of the ridge axis on a 10^4 yr. timescale, much wider than most visual estimates of the width of the neovolcanic zone but also integrating a longer period. The ARZ width agrees with the width of the zone of crustal emplacement estimates from the magnetic anomaly transition width and seismic layer 2A accumulation width. Excluding the lava flows from seamount volcanoes and the ARZ, smooth, highly reflective, off-axis lava fields are found on seafloor younger than ~0.2 Ma. The ~0.2 Ma corridor corroborates previous results from the distribution of small isolated volcanoes that indicates randomly distributed off-axis eruptions occur on crust younger than ~0.2 Ma.

1. Introduction

The nature of the relationship between tectonic segmentation and the volcanism at and near the ridge crest is important to understanding how ocean crust is constructed. Previous studies of crust-forming processes include seismic observations in corridors across the ridge [e.g., *Canales et al.*, 1998; *Carbotte et al.*, 1997; *Christeson et al.*, 1994], magnetic anomaly transition widths [e.g., *Macdonald*, 1977; *Macdonald et al.*, 1983; *Sempere and Macdonald*, 1986; *Sempere et al.*, 1987], geochemical trends inferred from areally-dense rock sampling [e.g., *Perfit and Chadwick*, 1998; *Reynolds and Langmuir*, 2000; *Sinton et al.*, 1991], and theoretical approaches [*Hooft et al.*, 1996]. These studies of crustal accretion at fast spreading ridges (>90 km/Myr full rate) generally have little discussion of the record of volcanism as it is laid out on the seafloor. The primary reason that the volcanic record has not been included is that investigation of volcanic processes at this scale requires the combination of small-scale observations and extensive coverage area, a difficult combination to achieve on the ocean floor. This study examines the near-ridge volcanism of the southern East Pacific Rise (SEPR) from 15°30'S to 19°S by merging fine-scale mapping along the ridge crest with HMR1 and SeaMARC II 12 kHz side-scan sonar data out to ~1 Ma crust to interpret how the relationship between volcanism and tectonic segmentation has varied over time.

The need for a better understanding of the variations in volcanic processes along the ridge is illustrated by the controversy over how tectonic segmentation relates to ridge magma supply. Axial segmentation of fast-spreading ridges appears to be related to crustal thickness variations [*Barth and Mutter*, 1996; *Canales et al.*, 1998; *Carbotte et al.*, 2000]. However, some studies suggest that magma supply, indicated by the robustness of the axial magma chamber, is unrelated to tectonic segmentation [*Hooft et al.*, 1997; *Kent et al.*, 2000]. *White et al.* [2000] found that ridge segmentation at the third-order scale corresponds to variations in lava effusion rate, and inferred disruptions in the axial magma plumbing system. This study expands upon the results of *White et al.* [2000], examining how ridge segmentation and volcanic processes relate over a much larger area (10^5 km^2) and broader range of axial discontinuities including OSCs and second order ridge segments.

Likewise, estimates of the across-axis width of volcanic layer emplacement differ widely depending upon the scale of observation, thus requiring additional constraints to help understand why these observations differ. Recent submersible mapping of lava flows on the SEPR suggests that typical ridge axis eruptions flow <2 km from the ridge axis and are not particularly voluminous in

comparison to basaltic eruptions at hotspots and slower spreading ridges [*Sinton et al.*, submitted; *Sinton et al.*, 1999]. Geophysical studies suggest that the volcanic layer increases in thickness most dramatically over a wider area, within 1-5 km of the ridge axis [*Carbotte et al.*, 1997; *Hooft et al.*, 1997; *Sempere et al.*, 1987]. Observations of off-axis lava fields and small volcanic edifices suggest the possibility that the emplacement of the volcanic layer may continue to >10 km off axis [*White et al.*, 1998].

Two types of volcanic terrain in the 12 kHz side-scan sonar imagery have not been investigated previously, but are common at the SEPR. One is the hummocky seafloor initially identified in relict overlapping spreading center (OSC) basins by *Cormier et al.* [1996]. The other is the smooth highly-reflective seafloor that has the characteristics of lava flow fields [e.g., *Macdonald et al.*, 1989]. Both of these terrain types are volcanically produced, and vastly different from the lineated, fault-bounded abyssal hills that are the most common type of terrain on the flanks of the SEPR [*Macdonald et al.*, 1996].

1.1 Regional Geological Context

Between the Garrett transform fault and the 20°40'S OSC, the axis of the SEPR forms a linear topographic high with a fairly uniform trend broken by five OSCs [*Scheirer et al.*, 1996a]. Previous studies of the SEPR have presented details of the tectonic history of the ridge [*Cormier and Macdonald*, 1994; *Cormier et al.*, 1996; *Lonsdale*, 1989], and described the distribution of the abundant off-axis volcanoes in the area [*Scheirer et al.*, 1996b; *Shen et al.*, 1995; *White et al.*, 1998]. The depth and cross-sectional area of the ridge axis in this area show one significant break at second-order OSC at 15°55'S [*Scheirer and Macdonald*, 1993]. This second-order OSC is the largest OSC in the study area, although the ridge axis is also offset by four left-stepping third-order OSCs (Figure 1). The third-order OSCs all correspond to gaps in the axial magma chamber (AMC) seismic reflector [*Detrick et al.*, 1993] and magmatic segment boundaries [*Sinton et al.*, 1991], but do not correspond to obvious long-wavelength changes in axial depth or cross-sectional area, proxies for the long-term axial magma budget [*Scheirer and Macdonald*, 1993]. *Cormier et al.* [1996] suggest that these OSCs were generated as a result of splitting of one larger OSC and are propagating along-axis at nearly three times the spreading rate.

The great number of RADs that have a well-known tectonic history make the SEPR at 16°-19°S an ideal place to relate off-axis seafloor morphology to similar morphology at the ridge where it has been studied at higher resolution. At the OSCs, the seafloor fabric is disrupted by the interaction of the two spreading centers as the curving OSC ridge tips are decapitated and rafted onto the ridge flanks by seafloor spreading [*Macdonald et al.*, 1984]. The steep, curved ridge tips at OSCs leave a trace of discordant lineaments away from the ridge axis that have been mapped in the backscatter side-scan and bathymetric data to determine the history of tectonic segmentation [*Cormier and Macdonald*, 1994; *Cormier et al.*, 1996].

Off-axis volcanism is common near the SEPR and can obscure some of the original volcanic fabric formed at the ridge axis. The extraordinarily abundant seamount chains on the west flank of the SEPR overprint the features formed at the ridge axis, but these mainly develop >10 km off-axis [*Scheirer et al.*, 1996b]. Far fewer seamount chains are found on the east flank of the ridge [*Scheirer et al.*, 1998]. Small isolated volcanoes are ubiquitous near the SEPR, but these do not obscure much area [*White et al.*, 1998].

1.2. Data Sources: HMR1, SeaMARC II, and DSL-120 Side-scan Sonar

This study focuses on the side-scan sonar backscatter imagery of volcanically produced seafloor fabric from the SEPR and its flanks, using extensive regional data collected by two near-surface towed 12 kHz side-scan systems. On R/V *Moana Wave* cruise 8710, the SeaMARC II sonar was used to map 18°-19°S in single-pass coverage on either side of the ridge axis [*Cormier and Macdonald*, 1994]. On R/V *Melville* cruise Gloria, leg 2, the HMR1 sonar was used to map 15°30'-18°S in overlapping swath coverage to obtain opposite look directions for the side-scan backscatter imagery for the map area [*Scheirer et al.*, 1996a]. We refer to these data collectively as the 12 kHz side-scan data throughout the rest of the paper. Both of the 12 kHz side-scan sonar systems have similar characteristics. The SeaMARC II has a swath width of ~10 km at 3000 m seafloor depth. The HMR1 has a corresponding swath width of ~20 km. Both systems have a practical resolution of 50-100 m pixels depending on the angle of incidence with the seafloor of the sonar sound and depth to the seafloor.

To achieve coverage at a much higher resolution than 12 kHz side-scan, the 120 kHz side-scan DSL-120 is towed ~100 m above the bottom to obtain backscatter imagery with ~1 m pixel resolution and bathymetry with ~5 m pixel resolution over a swath width of ~1 km along the ridge

crest. Features that are near the limit of resolution for the 12 kHz side-scan systems show up clearly in the DSL-120 sonar images, enhancing our sonar interpretation where coverage at two scales overlaps. Complete coverage of the ridge crest from 17°15'-18°40'S is available from DSL-120 surveys on *R/V Melville* cruise Sojourn, leg 2 [*White et al.*, 2000] and *R/V Atlantis* cruise 3, leg 31 [*Sinton et al.*, submitted; *Sinton et al.*, 1999].

The limits of available sonar coverage and the lack of identifiable volcanic fabric on older seafloor define the boundaries of our study area (Figure 1). On crust older than ~1 Ma, the mound fields become difficult to identify due to burial by sediment, and no more lava flow fields are observed. We have excluded from the study area much of the area dominated by seamount chains from 16° to 18°S west of the ridge axis, resulting in greater overall coverage of the east flank of the ridge (Figure 1). Volcanic fabric on the flanks of seamounts are probably related to seamount-forming eruptions rather than ridge axis volcanism and is discussed in previous work [*Scheirer et al.*, 1996b; *Shen et al.*, 1995]. Therefore, we do not consider the areas within the high-reflectivity sonar aprons of seamounts in this study. The study area boundaries include nearly equal coverage on both sides of the ridge axis out to ~20 km from the ridge axis enabling us to investigate the full history over >0.2 Ma and to ~1 Ma on the east flank.

2. Results

2.1. Detection of Volcanic Mounds in DSL-120 data Compared to SeaMARC II and HMR1 data

Where the 12 kHz side-scan and DSL-120 sonar coverage overlaps, the hummocky fabric in the 12 kHz data corresponds to small pillow mounds observed with DSL-120 sonar. Hummocky seafloor fabric, composed of many small mounds of sizes near the level of resolution of the 12 kHz side-scan backscatter, was noted in the relict OSC basins near the ridge axis prior to this study [*Cormier et al.*, 1996]. Hummocky fabric of the same nature was identified at the ridge axis near the OSCs. DSL-120 sonar surveys in 1996 [*White et al.*, 2000] and in 1999 [*Sinton et al.*, submitted; *White et al.*, 1999] revealed that the seafloor at these OSCs was densely covered with small volcanic mounds (Figure 2). Subsequent visual investigation found that these small volcanic mounds were composed primarily of pillow lava [*Sinton et al.*, submitted; *White et al.*, 2000]. The pillow mounds identified with DSL-120 have an average diameter of 200m diameter and height of 20m, and were classified as basaltic lava domes [*White et al.*, 2000]. The size of the average pillow mound is below

the resolution limit of the 12 kHz side-scan sonar, but the larger mounds or several mounds clustered closely together should be visible on 12 kHz records.

Volcanic mound fields identified from hummocky seafloor fabric in the 12 kHz side-scan records correspond to extensive areas of densely clustered pillow mounds that tend to form at OSCs. The mound fields have a minimum size cutoff of 3-4 km^2 due to the resolution of the 12 kHz sonar record. Pillow mounds are found in greatest extent and abundance at the OSCs, and although they increase in abundance near all third-order RADs, most of these areas are smaller than the minimum size cutoff for the identification of mound fields using 12 kHz surface-tow data (Figure 3). Along ~150 km of ridge crest surveyed with DSL-120, we found two areas of >4 km^2 that were densely covered in pillow mounds (Figure 3). Both of these areas are located at OSCs where volcanic mound fields are identified in the 12 kHz sonar records. At the one other OSC where overlapping DSL-120 and 12 kHz side-scan coverage exist, only a few pillow mounds were found in the DSL-120 data and mound fields near this OSC fall outside the coverage of the DSL-120 survey (Figure 3). The correlation of the mound fields with the areas where the DSL-120 pillow mounds cover at least 4 km^2 suggests that the hummocky 12 kHz side-scan return is due to the combined effect of many small mounds in the side-scan backscatter images.

To establish a detection threshold for individual mounds, we compare individual images of mounds in 12 kHz side-scan with individual pillow mounds in DSL-120 side-scan. The base outline of each mound in the DSL-120 survey was digitized, then projected onto digitized HMR1 and SeaMARC II side-scan records in a geographical information system. Allowing for geographical registration shifts of up to 200 m, we identified those mounds in the 12 kHz side-scan records that matched the location of a pillow mound in the DSL-120 records. Where a mound-like reflector was observed in the 12 kHz side-scan and no single matching pillow mound was found in the DSL-120 records, several small mounds may have blurred into one larger feature in the 12 kHz side-scan records. The 12 kHz side-scan systems are capable of detecting ~50% of pillow mounds with >60-70,000 m^2 base area or a basal diameter of ~300 m assuming that the mounds have circular bases. This base area appears to be the practical detection threshold for the 12 kHz sonar data. The percentage of pillow mounds detected declines rapidly for those with <60,000 m^2 basal area (Figure 4).

While the 12 kHz side-scan resolves the mound fields reliably, individual pillow mounds must be much larger than average to be seen in the 12 kHz side-scan. Overall, 16% of the mounds in the DSL-120 records have corresponding reflectors in the 12 kHz side-scan records. Some of these mounds are individuals outside the area defined by mound fields. The high backscatter reflectivity around the ridge axis in the 12 kHz side-scan records hampers the identification of small reflectors since the reflectivity contrast is very low, so that detection of mounds and mound fields is actually easier on the ridge flanks than on the crest. Because the detection of volcanic mound fields has proved reliable for areas >4 km^2 but individual mounds may be below the resolution threshold of the 12 kHz side-scan, we examine the off-axis record for volcanic mound fields rather than individual mounds.

2.2. Volcanic Mound Fields and Migration Paths of OSCs

Volcanic mound fields in the 12 kHz side-scan backscatter data are characterized by a hummocky seafloor fabric composed of many small mounds of fairly even size near the resolution limit of the 12 kHz side-scan. To define the mound fields, we traced their outlines on 1:100,000 SeaMARC II and 1:200,000 HMR1 maps of co-registered overlays of side-scan backscatter imagery and phase bathymetry. We chose mound fields somewhat conservatively, looking for areas of hummocky fabric large enough to be unambiguous. In areas less than 3-4 km^2 in the 12 kHz side-scan records, too few mounds were visible to define them as a mound field.

The discordant zones are areas of disturbed seafloor fabric surrounding the OSC migration traces identified by *Cormier et al.* [1996]. We picked the boundaries of the discordant zones based on the patterns of discordant lineaments (large scarps with trends not parallel to the abyssal hill fabric) and bathymetric anomalies (unusually deep grabens) [*Cormier et al.*, 1996], combined with an analysis of seafloor roughness. We expect higher scarps surrounding OSC fabric [*Cormier et al.*, 1996; *Crowder and Macdonald*, in press; *Goff et al.*, 1993]. Unusually deep grabens, very high fault scarps, and discordant lineaments all define distinct continuous swaths that we outlined to define the discordant zones (Figure 5).

The vast majority of the mound fields lie inside the discordant zones, and most of the others fall partly inside (Figure 6). Discordant zone boundaries picked entirely from tectonic criteria may miss some of the area affected by OSC migration processes because the volcanic mound fields often extend farther along the ridge axis than the overlap of the two ridge axes at the OSC [*White et al.*, 2000]. The discordant seafloor fabric is formed mainly where the two ridge axes overlap, but the

volcanic mound fields may be found in a much larger area surrounding the OSC (Figure 6). Mound fields found off-axis would be expected to often extend beyond the boundaries of the tectonically-defined discordant zone. If we assume that all of the mound fields that fall partially within the discordant zones should be included as part of that discordant zone, then the total area of mound fields within the discordant zone is ~2100 km^2 (Table 1). Otherwise the area of mound fields entirely within the defined discordant zone boundaries is ~1900 km^2. The mound fields also occupy a significant area of the discordant zones but a very minor area outside of them (Table 1).

Throughout the study area, the mound fields show no evidence of off-axis growth, remaining within one standard deviation of the mean mound field area (Figure 7). This is consistent with the formation of all of the mound fields near the rise axis, and subsequent passive rafting off-axis. Admittedly, we cannot detect if a few new individual mounds do form. However, if significant off-axis volcanism were common, it would likely produce large volcanic edifices consistently in discordant zones or result in a systematic increase in the size of the mound fields with distance from the ridge axis. Instead, the character of the mound fields remains very similar on- and off-axis. Additionally, the mound fields become difficult to identify from side-scan backscatter imagery on crust older than ~1 Ma (used as one of the constraints on our study area boundaries). Estimated sediment accumulation rates range widely, but a minimum of 2 cm/kyr [*Dekov and Kuptsov*, 1994; *Lyle et al.*, 1987; *Marchig et al.*, 1986] suggests that in ~1 Myr sediment thickness would have a significant effect on the relief of small (<20 m high) volcanic mounds, obscuring the entire mound field so long as no new mounds were forming. This evidence is also consistent with volcanic activity in the mound fields being limited to the immediate vicinity of the axial high.

Mound field size seems to be loosely related to the size of the OSC offset. For example, the largest mound field in our study area surrounds the large OSC at 15°55'S; very small mound fields are observed around the smallest OSCs at 16°30'S and 18°22'S. *Cormier et al.* [1996] infer that the sizes of OSCs within our study area probably decreased significantly at ~0.4 Ma, perhaps explaining why 3 of 5 outliers to the average size distribution of mound fields occur on crust older than 0.5 Ma.

2.3. Lava Fields

High reflectivity side-scan records over large flat areas and often obscuring small fault scarps have been interpreted as young lava flow fields [*Davis et al.*, 1986; *Fornari et al.*, 1985; *Macdonald et al.*, 1989]. Several similar lava fields exist within the study area, including a zone along the entire

length of the ridge axis. The double-coverage with the HMR1 north of 18°S simplifies lava field identification as lava fields will have high reflectivity from opposite ensonification directions, while steep slopes (fault scarps) will show up from just one direction. In utilizing the SeaMARC II data south of 18°S, more care must be taken to distinguish lava flows from seafloor slopes. In most cases, fault scarps appear as ribbons of high reflectivity that differ from the ameboid shapes of the lava fields.

A continuous zone of high-reflectivity backscatter side-scan surrounding the ridge axis makes up one long continuous lava field (Figure 8). We refer to this region as the axial reflective zone (ARZ). In the ARZ, re-paving by lava flows is so frequent that the seafloor is essentially sediment-free to the penetration depth of the sonar sound. The average width of the ARZ is ~7 km, varying from 5 to 10 km along most of the ridge axis (Figure 8). In some areas the ARZ is up to ~12 km wide, and north of 15°55'S the ARZ narrows to ~1 km width. Both ARZ width and axial cross-sectional area are small north of the 15°55'S OSC, and large around 17°30'S. We find no other correlation between ARZ width and ridge morphology, however ridge morphology is relatively uniform within the study area [*Scheirer and Macdonald*, 1993]. In particular, the ARZ width does not change systematically at OSCs.

The off-axis lava flow fields tabulated in this study are distinct areas of high-reflectivity 12 kHz side-scan outside of the ARZ that are neither part of seamount chains nor part of the apron around one of the isolated off-axis volcanoes (Figure 8) [*Scheirer et al.*, 1998; *Scheirer et al.*, 1996b; *White et al.*, 1998]. This criterion excludes most of the high-reflectivity seafloor, because most of it occurs around seamount volcanoes [*Scheirer et al.*, 1998; *Scheirer et al.*, 1996b]. The lava fields are all within ~15 km of the ridge axis on crust <0.2 Ma (Figure 8). Highly reflective lava fields are observed only within the same age range as the isolated near-axis volcanoes are inferred to form and grow [*White et al.*, 1998]. In many cases, the edges of lava fields terminate along an abyssal hill fault. Presumably, fault scarps dam and divert lava flows, indicating that this faulting preceded the lava flow emplacement.

All of the off-axis lava fields contain one or two small mound-like reflectors (Figure 9). However, these mounds are too small to show up as distinct off-axis volcanoes in SeaBeam2000 bathymetry [*White et al.*, 1998]. The small mounds within these lava fields may mark the source vents of the field. Off-axis volcanic eruptions are inferred to occur within 1-2 km of the axis based on the distinctive geochemical composition of the basalt [*Perfit et al.*, 1994; *Reynolds and Langmuir*, 2000].

Alternatively, they may be rootless volcanic structures formed by lava flow inflation or break-outs from lava tubes. Further studies will be necessary to resolve ambiguities about the origin of these extensive lava fields.

We find that 7 of 14 lava fields that are contiguous with the ARZ, originating on the axial topographic high and protruding onto lower reflectivity (older) seafloor. These contiguous lava fields are differentiated from the ARZ by having higher reflectivity than the surrounding seafloor at the edge of the ARZ, and by their irregular outline tending to flow between abyssal hills. We are unable to trace any of them back to the ridge axis due to insufficient reflectivity contrast. The contiguous lava fields may be evidence of rare large eruptions from the ridge axis. Including the contiguous lava fields, lava flows may travel >20 km from the vent, but rarely reach more than 10 km away perpendicular to the axis because the lava tends to flow along axis-parallel grabens.

3. Discussion

3.1. Across-Axis Width of Volcanic Emplacement

Frequent volcanic activity seems to continue out to a crustal age of 0.2 Ma on the SEPR. This crustal age limit, corresponding to a distance of ~15 km off-axis, is the zone where lava fields are found, isolated off-axis volcanoes form, and most seamount chains initiate [*Scheirer et al.*, 1996b; *White et al.*, 1998]. The <0.2 Ma crust zone of frequent, isolated eruptions was found to apply independent of spreading rate for the northern EPR [*Alexander and Macdonald*, 1996] and Mid-Atlantic Ridge [*Smith and Cann*, 1999], suggesting that lithospheric penetrability may control off-axis eruptions [*White et al.*, 1998]. Mound fields appear to form on-axis, and we have found no evidence that they contribute to off-axis volcanism. On the other hand, lava fields locally resurface large areas outside the ARZ (Figure 8). On crust younger than 0.2 Ma, lava fields, isolated volcanoes, and seamount chains together resurface up to 8-10% of the seafloor outside of the area of the ARZ. Excluding the ARZ, the lava fields alone resurface a total area of 250-260 km^2 (~3% of the seafloor) although they create no edifices within the resolution limits of multibeam bathymetry. The lava fields individually cover areas ranging from 1 to 45 km^2 with an average area of 16 km^2 which is an order of magnitude smaller than the 220 km^2 lava field mapped at 8°S on the EPR [*Macdonald et al.*, 1989]. Although off-axis eruptions can be quite extensive, the large eruptions seem to be unusual and do not systematically thicken the crust (except at seamounts). Thus, the vast majority of the oceanic crust is formed within the ARZ.

The ARZ width agrees closely with the width of volcanic layer thickening inferred from seismic and magnetic measurements, while estimates of the neovolcanic zone width from visual observations are much narrower. The ARZ width is typically 5-10 km, considerably wider than the 0.5-2 km wide neovolcanic zone estimated from visual observations [*Auzende et al.*, 1996; *Sinton et al.*, 1999; *White et al.*, 2000]. The seismic record in our study area indicates that the thickening of seismic layer 2A takes place over a 2-7 km wide zone but varies in width over short (10 km) distances along-axis [*Carbotte et al.*, 1997; *Hooft et al.*, 1997; *Hooft et al.*, 1996]. The magnetic anomaly transition widths measured from the near-bottom field at the SEPR also suggest that crustal accretion takes place in a 3-4 km wide zone, but that surface flows may cover a region 4-10 km wide [*Sempere et al.*, 1987].

The measured width of the ARZ in 12 kHz side-scan records may be ~1 km wider than the distance over which the extrusive layer thickens by frequent lava flows, due to the sediment penetration capability of 12 kHz sonar. Sedimentation rates near the SEPR and volume scattering induced by sub-bottom penetration of the 12 kHz side-scan signal are both highly variable and poorly constrained, therefore we estimate the lava flow emplacement in the ARZ as ranges of values. Assuming a sedimentation rate between 2-10 cm/kyr. [*Dekov and Kuptsov*, 1994; *Lyle et al.*, 1987; *Marchig et al.*, 1986] and that less than 10-50 cm of sediment is effectively transparent to 12 kHz side-scan [*Davis et al.*, 1986; *Nishimura*, 1997; *Tyce*, 1986], the ARZ full width should be limited to 1-3 km at the 14.5 cm/yr full spreading rate [*Cormier et al.*, 1996] if only the ridge axis was covered in "Age 0" unsedimented lava. An ARZ width of 5-10 km implies that Age 0 lava covers a 2-9 km zone (total width). Near 17°30'S where the ARZ is 10-11 km wide, Age 0 lava extends ~2-5 km off-axis. In the same area, *Carbotte et al.* [1997] found seismic layer 2A continued to thicken up to >4 km off axis. The 2-9 km wide zone of Age 0 lava flows from these simple calculations based on ARZ width agrees with the 4-10 km width of surface lava flows suggested from magnetic polarity transition boundary offsets on the SEPR [*Sempere et al.*, 1987].

The time-integrated view of lava flows in the ARZ may reconcile the width of volcanic layer thickening indicated by magnetic and seismic measurements with the width of lava flow emplacement. The ARZ yields a time-integrated view of volcanism over several thousand years due to the sediment penetration capability of 12 kHz sonar. Assuming the same sedimentation rate and sediment transparency used earlier, the minimum recurrence interval for >2 km long lava flows is 1-25 kyr. to

maintain a >4 km wide ARZ. In comparison, the neovolcanic zone estimated from visual observations of glassy, nearly unsedimented lava flows may integrate the volcanic activity over just a few hundred years or less [*CYAMEX*, 1981; *Haymon et al.*, 1993].

The discrepancy between the width of the ARZ and the visual estimate of the neovolcanic zone, combined with the presence of long lava fields contiguous with ARZ suggest that the SEPR has two distinct eruptive styles: 1) short, low volume, and frequent; and 2) long, high volume, and rare. Modeling crustal emplacement to fit the shape of the base of seismic layer 2A on the SEPR, *Hooft et al*. [1996] found the best match was a bimodal distribution lava flow lengths with 95% of lava flows ~50 m long and 5% of lava flows emplaced 0.5 km off-axis and ~1 km long. *Hooft et al*. [1996] predict that a >1 km long lava flow should occur every 10^2-10^3 yr. given an interval of 10^1 yr. between eruptions on the SEPR. We infer a similarly short recurrence interval of 10^3-10^4 yr. for lava flows to re-pave the width of the ARZ. In fact, recent lava flows of >1 km length have been found near collapse trough/lava lakes suggesting that flows of such length are not particularly rare on the SEPR [*Sinton et al.*, submitted; *White et al.*, 2000]. The idea that eruptive behavior of the EPR may be bimodal is also implied in multi-stage models for the formation of axial summit troughs [*Fornari et al.*, 1998; *Lagabrielle and Cormier*, 1999]. The lava flow fields, especially those contiguous with the ARZ, are possible evidence for rare voluminous eruptions from the SEPR. Unfortunately, we cannot distinguish between long and short flows within the ARZ; because, most lava flows within the ARZ look equally young on the 12 kHz backscatter sonar images. Further work defining and mapping products of individual eruptions is needed to accurately determine a size:frequency ratio for mid-ocean ridge eruptions.

3.2. Indications of Along-Axis Volcanic Segmentation

The close association of mound fields and discordant zones from second- and third-order OSCs in the 12 kHz side-scan records corroborates previous observations that eruptions of pillow lava are common at third-order RADs [*White et al.*, 2000], and expands these data to include second-order RADs as well (note that the end of a third-order segment may be a second-order ridge discontinuity, see figure 2 in *Macdonald et al.* [1991]). At the axis, OSCs are the exclusive location of extensive (>4 km^2) areas covered by pillow mounds (Figure 3). Mound fields are also ubiquitous within the discordant zones and quite rare outside of them (Table 1). The longevity of the OSC offsets allows the discordant tectonic fabric and volcanic mound fields to be preserved off-axis without being

overprinted by subsequent volcanism within the ARZ. Although pillow mounds occur at all of the third-order RADs on the SEPR, apparently only the OSCs have sufficient size and longevity to create mound fields large enough to be identified (>4 km^2) on 12 kHz side-scan records. None of the other RADs have sufficient size or longevity to leave a detectable off-axis trace. The discordant zones we identified suggest that 20-25% of the seafloor in the study area is disrupted by volcanic and tectonic processes related to OSCs.

The volcanic mounds at OSCs imply that eruptions tend to have lower effusion rates near OSCs than elsewhere along the ridge. The pillow mounds comprising each mound field are inferred to form at very low lava effusion rates [*Bonatti and Harrison*, 1988; *Gregg and Fink*, 1995; *Griffiths and Fink*, 1992; *White et al.*, 2000]. Outside of the areas of pillow mounds near the second- and third-order RADs, the higher effusion rate lobate lava flows are generally the most common lava morphology on the SEPR [*Auzende et al.*, 1996; *Renard et al.*, 1985; *Sinton et al.*, submitted; *White et al.*, 2000]. The occurrence of mound fields around OSCs is not unique to the SEPR, but has been noted in high-resolution studies of OSCs on the northern EPR as well [*Antrim et al.*, 1988; *Hekinian et al.*, 1985; *Macdonald et al.*, 1992; *Sempere and Macdonald*, 1986]. The SeaMARC II data from 9º-10ºN also shows mound fields in both the overlap basin and the migration trace of the 9º03'N OSC [*Macdonald et al.*, 1992; *Sempere and Macdonald*, 1986].

One possible factor contributing to the inferred reduction in eruption effusion rates is the decrease in spreading rate on the ridge axes within OSCs. The spreading rate at the ridge axis on each limb of the OSC decreases because the sum of the spreading rate for both spreading centers in the overlap zone must not be greater than the total plate opening rate. Because the seafloor just beyond the OSC rift tip is not spreading at all, but the ridge axis behind the OSC is rifting at the total spreading rate, the spreading rate along the OSC limb must decrease approaching the OSC tip [*Macdonald et al.*, 1984]. In effect, each limb of the OSC acts as a slower spreading-rate ridge axis [*Macdonald et al.*, 1988]. The inferred link between lava effusion rate and spreading rate at OSCs on the EPR resembles the global relationship between lava morphology and spreading rate. Slow-spreading ridges seem to erupt more pillow lava than fast-spreading ridges (e.g.,[*Perfit and Chadwick*, 1998]). High-resolution DSL-120 data show that the number of pillow mounds increases from mid-segment to segment end outside of the region where the opposing limbs of an OSC overlap. The link

between spreading rate and lava morphology cannot explain the mound fields that extend along the ridge axis beyond the overlap zone between the two ridge axes.

Disruptions to the shallow magma delivery system, manifested by breaks in the AMC, may explain the development of mound fields at OSCs. The absence of a steady-state AMC is common to both slow-spreading ridges and OSCs on the EPR [*Detrick et al.*, 1987; *Detrick et al.*, 1993; *Detrick et al.*, 1990]. Petrologic data also suggest that separate, disconnected magma chambers exist on either side of the OSCs in our study area [*Sinton et al.*, 1991]. On the EPR, the disappearance of the AMC at RADs is often accompanied by an increase in crustal thickness [*Barth and Mutter*, 1996; *Canales et al.*, 1998; *Cormier et al.*, 1995; *Scheirer et al.*, 1998]. These changes in crustal structure affect a region much larger than the overlap between the two ridge axes at OSCs. Disruptions to the AMC appear correlated with existence of pillow mounds where both data coexist [*White et al.*, 2000]. The lack of a steady-state AMC may indicate a lower magma pressure and thicker brittle lid, leading to a reduction in the width of eruptive dikes. Small changes in dike width can produce large changes in the lava effusion rate at eruption, controlling the overall morphology of volcanic vent structures [*Head et al.*, 1996]. Also, a reduction in magma pressure will lead to lower volcanic effusion rates for any dike width. The predominance of pillow lava and pillow mounds on the EPR in areas where an AMC is not detected suggests that magma delivery is generally impeded at OSCs relative to the mid-segment regions.

3.3. Evidence for the Linkage of Tectonic, Magmatic, and Volcanic Segmentation

Our results suggest that mound fields coincide with major disruptions to the axial volcanic system inferred from the structural and magmatic segmentation of the ridge axis that occurs at OSCs [*Sinton and Detrick*, 1992; *Sinton et al.*, 1991] (Figure 6). The areas of the mound fields do not increase over time or distance from the ridge axis implying that mound fields form at the ridge axis and are not volcanically active away from the ridge axis (Figure 7). Thus, mound fields found off-axis are most likely relict features of past disruptions to the axial volcanic system. These disruptions to the axial volcanic system have occurred at OSCs within the study area for the last 1 Myr (Figure 5).

Tectonic, magmatic, and volcanic segment boundaries all coincide in the study area to within the limits of the resolution of each dataset. These datasets indicate the locations of ridge discontinuities from three independent measurements. *Cormier et al.* [1996] and *Scheirer et al.* [1996a] describe the tectonic segmentation of the ridge based on the morphological and structural

criteria of *Macdonald et al.* [1988]. Only the segments bounded by OSCs were included, although the segment locations were chosen from multibeam bathymetry maps with a spatial resolution of ~100 m. *Sinton et al.* [1991] define magmatic segments based on the along-axis continuity of volcanic glass samples with similar parental magmas. Samples from dredges made 10-15 km apart along-axis were used to define magmatic segmentation, limiting the resolution to segments >20 km long. This spacing eliminates most of the more subtle third-order discontinuities, but not the longer OSC-bounded segments. The volcanic segmentation is inferred from the distribution of volcanic mound fields as an extension of the pillow mounds found in DSL-120 sonar data [*White et al.*, 2000]. The 12 kHz surface-tow sonar appears to resolve mound fields >4 km^2 in area. This level of resolution also eliminates most of the more subtle third-order discontinuities, but not the OSCs. This result suggests that the segmentation of the magma supply to the ridge axis is closely linked to the morphological segmentation of the ridge.

4. Conclusions

Eruptive processes are strongly linked to ridge segmentation at super-fast spreading rates based on HMR1 and SeaMARC II side-scan sonar data from the SEPR. Our primary results concern the close association of volcanic mound fields with OSCs, and the significance of isolated off-axis lava fields.

1. The hummocky seafloor fabric in HMR1 and SeaMARC II side-scan sonar is caused by fields of volcanic mounds. These mound fields form near the axis, and have been imaged there with the DSL-120 sonar as extensive, dense clusters of small volcanic mounds. The mound fields within the neovolcanic zone are located at volcanic segment ends.
2. The areas of the mound fields do not increase with age or distance from the ridge axis implying that mound fields are formed at the ridge axis, within the ARZ, and do not commonly continue to be volcanically active away from the ridge axis. Axial pillow mounds do not commonly evolve into larger volcanoes but rather manifest a disruption in the axial structure corresponding to the magmatic segmentation defined by *Sinton et al.* [1991]. The lack of mound fields outside OSC discordant zones suggests that the present association between the segmentation of the volcanic systems and ridge axis morphology has been maintained through time. Off-axis volcanoes and seamounts initiate independently of the pillow mounds.

3. Volcanic mound fields are inferred to form as a result of decreased volcanic effusion rates around volcanic segment ends (second or third order RADs) on the SEPR. The close association of mound fields with discordant zones illustrates that the effusion rate systematically decreases at RADs that are large enough to leave an off-axis discordant zone.
4. Tectonic, magmatic, and volcanic segment boundaries all coincide within the study area. Each set of segment boundaries were defined based on independent data. The agreement of the tectonic, magmatic, and volcanic record on the locations of ridge discontinuities at OSCs suggests that magma supply and ridge structure are closely linked.
5. Isolated, off-axis lava fields are patches of highly reflective seafloor in the SeaMARC II and HMR1 sonar data. Lava fields occur only on crust <0.2 Ma, within the same zone where isolated off-axis volcanoes form and grow [*White et al.*, 1998] and most seamount chains initiate [*Scheirer et al.*, 1996b]. Random off-axis eruptions appear to be commonplace on the flanks of the SEPR on <0.2 Ma crust. However, these off-axis eruptions probably add very little volume to the oceanic crust.
6. The ARZ is an area of nearly uniform high-reflectivity seafloor surrounding the ridge axis corresponding to the width of volcanic activity integrated over several thousand years. Its changes in width are not systematically correlated to the RADs. Occasional lava flows may reach up to 7 km off axis. However, the full width of the ARZ is typically 5-10 km. The width of the ARZ is in close agreement with the width of the zone of crustal accretion estimated from seismic layer 2A thickening and magnetic anomaly transition widths [*Carbotte et al.*, 1997; *Sempere et al.*, 1987].

References

Alexander, R.T., and K.C. Macdonald, Small off-axis volcanoes on the East Pacific Rise, *Earth Planet. Sci. Lett.*, *139*, 387-394, 1996.

Antrim, L., J.-C. Sempere, K.C. Macdonald, and F.N. Spiess, Fine scale study of a small overlapping spreading center system at 12°54'N on the East Pacific Rise, *Mar. Geophys. Res.*, *9*, 115-130, 1988.

Auzende, J.M., V. Ballu, R. Batiza, D. Bideau, J.L. Charlou, M.-H. Cormier, Y. Fouquet, P. Geistdoerfor, Y. Lagabrielle, J. Sinton, and P. Spadea, Recent tectonic, magmatic and hydrothermal activity on the East Pacific Rise between 17° and 19°S: Submersible observations, *J. Geophys. Res.*, *101*, 17,995-18,010, 1996.

Barth, G.A., and J.C. Mutter, Variability in oceanic crustal thickness and structure: Multichannel seismic reflection results from the northern East Pacific Rise, *J. Geophys. Res.*, *101*, 17,951-17,975, 1996.

Bonatti, E., and C.G.A. Harrison, Eruption style of basalt in oceanic spreading ridges and seamounts: Effect of magma temperature and viscosity, *J. Geophys. Res.*, *93*, 2967-2980, 1988.

Canales, J.P., R.S. Detrick, S. Bazin, A.J. Harding, and J.A. Orcutt, Off-axis crustal thickness across and along the East Pacific Rise within the MELT area, *Science*, *280*, 1218-1220, 1998.

Carbotte, S.M., J.C. Mutter, and L. Xu, Contribution of volcanism and tectonism to axial and flank morphology of the southern East Pacific Rise, 17°10'-17°40'S, from a study of layer 2A geometry, *J. Geophys. Res.*, *102* (B5), 10,165-10184, 1997.

Carbotte, S.M., A. Solomon, and G. Ponce-Correa, Evaluation of morphological indicators of magma supply and segmentation from a seismic reflection study of the East Pacific Rise, 15 30'-17 N, *J. Geophys. Res.*, *105* (B2), 2737-2760, 2000.

Christeson, G.L., G.M. Purdy, and G.J. Fryer, Seismic constraints on shallow crustal emplacement processes at the fast spreading East Pacific Rise, *J. Geophys. Res.*, *99* (B9), 17,957-17,973, 1994.

Cormier, M.H., K.C. Macdonald, and D.S. Wilson, A three-dimensional gravity analysis of the East Pacific Rise from 18°-21°30'S., *J. Geophys. Res*, *100*, 8063-8082, 1995.

Cormier, M.-H., and K.C. Macdonald, East Pacific Rise 18°S-19°S: Asymmetric spreading and ridge reorientation by ultra-fast migration of ridge axis discontinuities, *J. Geophys. Res.*, *99*, 543-564, 1994.

Cormier, M.-H., D.S. Scheirer, and K.C. Macdonald, Evolution of the East Pacific Rise at 16°-19°S since 5 Ma: Bisection of OSCs by new rapidly propagating ridge segments, *Mar. Geophys. Res*, *18*, 52-84, 1996.

Crowder, L.K., and K.C. Macdonald, New constraints on the width of the zone of active faulting on the East Pacific Rise 8 30'N- 10 N from Sea Beam bathymetry and SeaMARC II side-scan sonar, *Mar. Geophys. Res.*, *In Press*, 2001.

CYAMEX, First manned submersible dives on the East Pacific Rise at 21°N (Project RITA): General results, *Mar. Geophys. Res.*, *4*, 345-379, 1981.

Davis, E.E., R.G. Currie, B.S. Sawyer, and J.G. Kosalos, The use of swath bathymetric and acoustic image mapping tools in marine geoscience, *Mar. Technol. Soc.*, *20*, 17-27, 1986.

Dekov, V.M., and V.M. Kuptsov, Late quarternary rates of accumulation of metal-bearing sediments on the East Pacific Rise, *Oceanology*, *32*, 94-101, 1994.

Detrick, R.S., P. Buhl, E. Vera, J. Mutter, J. Orcutt, J. Madsen, and T. Brocher, Multi-channel seismic imaging of a crustal magma chamber along the East Pacific Rise, *Nature*, *326*, 35-41, 1987.

Detrick, R.S., A.J. Harding, G.M. Kent, J.A. Orcutt, J.C. Mutter, and P. Buhl, Seismic structure of the Southern East Pacific Rise, *Science*, *259*, 499-503, 1993.

Detrick, R.S., J.C. Mutter, P. Buhl, and I.I. Kim, No evidence from multichannel reflection data for a crustal magma chamber in the MARK Area on the Mid-Atlantic Ridge, *Nature*, *347*, 61-63, 1990.

Fornari, D.J., R.M. Haymon, M.R. Perfit, T.K.P. Gregg, and M.H. Edwards, Axial summit trough of the East Pacific Rise 9°N to 10°N: Geological characteristics and evolution of the axial zone on fast-spreading mid-ocean ridges, *J. Geophys. Res.*, *103*, 9827-9855, 1998.

Fornari, D.J., W.B.F. Ryan, and P.J. Fox, Sea-floor lava fields on the East Pacific Rise, *Geol.*, *13*, 413-416, 1985.

Goff, J.A., A. Malinverno, D.J. Fornari, and J.R. Cochran, Abyssal hill segmentation: Quantitative analysis of the East Pacific Rise Flanks 7°S-9°S, *J. Geophys. Res.*, *98*, 13851-13862, 1993.

Gregg, T.K.P., and J.H. Fink, Quantification of submarine lava-flow morphology through analog experiments, *Geology*, *23*, 73-76, 1995.

Griffiths, R.W., and J.A. Fink, Solidification and morphology of submarine lavas; a dependence on extrusion rate, *J. Geophys. Res.*, *97* (B13), 19729-19737, 1992.

Haymon, R.M., and, and others, Volcanic eruption of the mid-ocean ridge along the East Pacific Rise crest at 9°45'-52'N: Direct submersible observations of seafloor phenomena associated with an eruption event in April, 1991, *Earth Planet. Sci. Lett.*, *119*, 85-101, 1993.

Head, J.W., L. Wilson, and D.K. Smith, Mid-ocean ridge eruptive vent morphology and substructure: Evidence for dike widths, eruption rates, and the evolution of eruptions and axial volcanic ridges, *J. Geophys. Res.*, *101* (B12), 28,265-28,280, 1996.

Hekinian, R., J.M. Auzende, J. Francheteau, P. Gente, W.B.F. Ryan, and E.S. Kappel, Offset spreading centers near 12 53'N on the East Pacific Rise: Submersible observations and composition of the volcanics, *Mar. Geophys. Res.*, *7* (3), 329-358, 1985.

Hooft, E.E., R.S. Detrick, and G.M. Kent, Seismic structure and indicators of magma budget along the Southern East Pacific Rise, *J. Geophys. Res.*, *102* (B12), 27319-27340, 1997.

Hooft, E.E.E., H. Schouten, and R.S. Detrick, Constraining crustal emplacement processes from the variation in seismic layer 2A thickness at the East Pacific Rise, *Earth Planet. Sci. Lett.*, *142*, 289-309, 1996.

Kent, G.M., S.C. Singh, A.J. Harding, M.C. Sinha, J.A. Orcutt, P.J. Barton, R.S. White, S. Bazin, R.W. Hobbs, C.H. Tong, and J.W. Pye, Evidence from three-dimensional seismic reflectivity images for enhanced melt supply beneath mid-ocean ridge discontinuities, *Nature, 406*, 614-618, 2000.

Lagabrielle, Y., and M.-H. Cormier, Formation of large summit troughs along the East Pacific Rise as collapse calderas: An evolutionary model, *J. Geophys. Res., 104*, 12,971-12,988, 1999.

Lonsdale, P., Segmentation of the Pacific-Nazca spreading center, 1°N-20°S, *J. Geophys. Res., 94*, 12197-12226, 1989.

Lyle, M., M. Leinen, R.M. Owen, and D.K. Rea, Late Tertiary history of hydrothermal deposition at the East Pacific Rise, 19°S: Correlation to volcano-tectonic events, *Geophys. Res. Lett., 14*, 595-598, 1987.

Macdonald, K.C., Near-bottom magnetic anomalies, asymmetric spreading, oblique spreading, and tectonics of the Mid-Atlantic Ridge near lat 37N, *Geol. Soc. Am. Bull., 88*, 541-555, 1977.

Macdonald, K.C., The East Pacific Rise south of Garrett: Volcanic activity predicted for 14°-14°30'S, *EOS Trans. AGU, 72*, 506, 1991.

Macdonald, K.C., P.J. Fox, R.T. Alexander, R. Pockalny, and P. Gente, Volcanic growth faults and the origin of Pacific abyssal hills, *Nature, 380*, 125-129, 1996.

Macdonald, K.C., P.J. Fox, S. Carbotte, M. Eisen, S. Miller, L. Perram, D. Scheirer, S. Tighe, and C. Weiland, The East Pacific Rise and its flanks, 8°-18°N: History of segmentation, propagation and spreading direction based on SeaMARC II and Sea Beam studies, *Mar. Geophys. Res., 14*, 299-344, 1992.

Macdonald, K.C., P.J. Fox, L.J. Perram, M.F. Eisen, R.M. Haymon, S.P. Miller, S.M. Carbotte, M.-H. Cormier, and A.N. Shor, A new view of the mid-ocean ridge from the behaviour of ridge-axis discontinuities, *Nature, 335*, 217-225, 1988.

Macdonald, K.C., R. Haymon, and A. Shor, A 220 km2 recently erupted lava field on the East Pacific Rise near lat 8°S, *Geology, 17*, 212-216, 1989.

Macdonald, K.C., S.P. Miller, B.P. Luyendyk, T.M. Atwater, and L. Shure, Investigation of a Vine-Matthews magnetic lineation from a submersible: The source and character of marine magnetic anomalies, *J. Geophys. Res., 88*, 3403-3418, 1983.

Macdonald, K.C., J.-C. Sempere, and P.J. Fox, East Pacific Rise from Siqueiros to Orozco Fracture Zones: Along-strike continuity of axial neovolcanic zone and structure and evolution of overlapping spreading centers, *J. Geophys. Res., 89*, 6049-6069, 1984.

Marchig, V., J. Erzinger, and P.M. Heinze, Sediment in the black smoker area of the East Pacific Rise, *Earth Planet. Sci. Lett., 79*, 93-106, 1986.

Nishimura, C.E., *Fundamentals of acoustic backscatter imagery.*, 67 pp., Naval Research Laboratory, Washington, D.C., 1997.

Perfit, M.R., and W.W. Chadwick, Magmatism at mid-ocean ridges: constraints from volcanological and geochemical investigations, in *Faulting and magmatism at mid-ocean ridges*, edited by W.R. Buck, P.T. Delaney, J.A. Karson, and Y. Lagabrielle, pp. 59-116, AGU, Washington DC, 1998.

Perfit, M.R., D.J. Fornari, M.C. Smith, J.F. Bender, C.H. Langmuir, and R.M. Haymon, Small-scale spatial and temporal variations in mid-ocean ridge crest magmatic processes, *Geology*, *22*, 375-379, 1994.

Renard, V., R. Hekinian, J. Francheteau, R.D. Ballard, and H. Backer, Submersible observations at the axis of the ultra fast spreading East Pacific Rise (17°30' to 21°30'S), *Earth Planet. Sci. Lett.*, *88*, 339-353, 1985.

Reynolds, J.R., and C.H. Langmuir, Identification and implications of off-axis lava flows around the East Pacific Rise, *Geochem. Geophys. Geosys.*, *1*, 2000.

Scheirer, D.S., D.W. Forsyth, M.-H. Cormier, and K.C. Macdonald, Shipboard Geophysical Indications of Asymmetry and Melt Production Beneath the East Pacific Rise near the MELT Experiment, *Science*, *280*, 1221-1224, 1998.

Scheirer, D.S., and K.C. Macdonald, Variation in cross-sectional area of the axial ridge along the East Pacific Rise: Evidence for the magamatic budget of a fast-spreading center, *J. Geophys. Res.*, *98*, 7871-7885, 1993.

Scheirer, D.S., K.C. Macdonald, D.W. Forsyth, S.P. Miller, D.W. Wright, and M.-H. Cormier, A map series of the southern East Pacific Rise and its flanks, 15°S to 19°S, *Mar. Geophys. Res.*, *18*, 1-12, 1996a.

Scheirer, D.S., K.C. Macdonald, D.W. Forsyth, and Y. Shen, Abundant seamounts of the Rano Rahi seamount field near the southern East Pacific Rise, 15º to 19ºS, *Mar.Geophys.Res.*, *18*, 13-52, 1996b.

Sempere, J.-C., and K.C. Macdonald, Deep-Tow studies of the overlapping spreading centers at 9°03'N on the East Pacific Rise, *Tectonics*, *5*, 881-900, 1986.

Sempere, J.-C., K.C. Macdonald, S.P. Miller, and L. Shure, Detailed study of the Brunhes/Matuyama reversal boundary on the East Pacific Rise at 19°30'S: Implications for crustal emplacement processes at an ultra fast spreading center, *Mar. Geophys. Res.*, *9*, 1-23, 1987.

Shen, Y., D.S. Scheirer, D.W. Forsyth, and K.C. Macdonald, Trade-off in production between adjacent seamount chains near the East Pacific Rise, *Nature*, *373*, 140-143, 1995.

Sinton, J., E. Bergmanis, K. Rubin, R. Batiza, T.K.P. Gregg, K. Gronvold, K. Macdonald, and S. White, Volcanic eruptions on mid-ocean ridges: New evidence from the superfast-spreading East Pacific Rise, 17-19S, *J. Geophys. Res., in review*, 2001.

Sinton, J.M., R. Batiza, K. Rubin, T. Gregg, E. Bergmanis, K. Gronvold, S. White, K. Macdonald, M. Cormier, A. Shah, and W. Ryan, Volcanic eruptions at superfast spreading mid-ocean ridges: Lava flows on the East Pacific Rise, 17-19 S, *Eos, Trans. AGU., 80* ((46), Fall Meet. Suppl.), F1097, 1999.

Sinton, J.M., and R.S. Detrick, Mid-ocean ridge magma chambers, *J. Geophys. Res., 97* , 197-216, 1992.

Sinton, J.M., S.M. Smaglik, J.J. Mahoney, and K.C. Macdonald, Magmatic processes at superfast spreading mid-ocean ridges: Glass compositional variations along the East Pacific Rise 13°-23°S, *J. Geophys. Res., 96*, 6133-6155, 1991.

Smith, D.K., and J.R. Cann, Constructing the upper crust of the Mid-Atlantic Ridge: A reinterpretation based on the Puna Ridge, Kilauea Volcano, *J. Geophys. Res., 104*, 25,379-25,400, 1999.

Tyce, R.C., Deep seafloor mapping systems-A review, *Mar. Tech. Soc. J., 20*, 4-16, 1986.

White, S.M., K.C. Macdonald, and R.M. Haymon, Basaltic lava domes, lava lakes, and volcanic segmentation of the southern East Pacific Rise, *J. Geophys. Res., 105*, 23,519-23,536, 2000.

White, S.M., K.C. Macdonald, R.M. Haymon, and J.M. Sinton, Volcanic segmentation of the SEPR revealed by regional along-strike changes in lava morphology, *Eos, Trans. Am. Geophys. U., 80* (46 (Fall Meet. Suppl.)), F1097, 1999.

White, S.M., K.C. Macdonald, D.S. Scheirer, and M.-H. Cormier, Distribution of isolated volcanoes on the flanks of the East Pacific Rise, 15.3º-20ºS, *J. Geophys. Res., 103*, 30,371-30,384, 1998.

Figure Captions

Figure 1. Shaded-relief bathymetry, false-illuminated from the northwest, showing the ridge axis, large off-axis volcanoes, and seafloor fabric in and surrounding the study area. Solid black line outlines the boundary of the study area. Along the ridge axis, the DSL-120 survey swath is outlined. Each of the overlapping spreading centers is labeled "OSC" to the right of the ridge. Arrows point to ends of magmatic segments (L-H) defined by *Sinton et al.* [1991]. Seamount chains overprint most of the seafloor just outside the study area from 17ºS to 18ºS. An example of anomalous abyssal hill fabric can be seen near the edge of the survey area at 17ºS. Map inset shows the survey area location in the context of the local oceanic plates.

Figure 2. Comparison of the mound fields resolved by 12 kHz side-scan to the pillow mounds in the DSL-120 side-scan records at the 18°35'S OSC. Backscatter side-scan from SeaMARC II (left panel), and DSL-120 (right panel), and our sonar interpretations of each dataset (middle panel). Higher backscatter reflectivity is darker. The ridge axis is marked by double line. In the middle panel, axial pillow mounds identified on the DSL-120 record are shown as black areas, and the mound fields from SeaMARC II are shaded gray areas. The dashed line outlines the DSL-120 swaths from the right panel. The greatest concentration of large pillow mounds in DSL-120 records occur where mound fields are identified in the SeaMARC II records, around the east limb and south of the west limb of the OSC. In areas marked "A" and "B", individual pillow mounds are barely detectable in the SeaMARC II records, but do not form part of a recognizable mound field of >4 km^2 area (see text for discussion).

Figure 3. The locations of DSL-120 sonar coverage within the study area. A double line traces the ridge axis, and dashed lines outline the area of DSL-120 sonar coverage. Each small open circle represents one pillow mound identified from DSL-120 data. The mound fields identified from 12 kHz side-scan are shaded gray areas. The minimum size of the mound fields we identified is ~4 km^2 based on the resolution of the 12 kHz side-scan records. All >4 km^2 groups of pillow mounds in DSL-120 data correspond to mound fields visible in 12 kHz side-scan. Some of the largest pillow mounds identified in DSL-120 data were also visible in the 12 kHz side-scan as isolated features. Mound fields were found at all of the OSCs. However, the 18°20'S OSC is only sparsely covered by pillow mounds observed in the DSL-120 data and mound fields were detected in the 12 kHz side-scan only outside the DSL-120 coverage area.

Figure 4. Graph showing how many individual pillow mounds in the DSL-120 record were also detected in the 12 kHz side-scan. Pillow mounds are binned by 10,000 m^2 base area increments up to the maximum size shown on the x-axis. The shaded bars show the number detected with DSL-120 coverage, and the cross-hashed bars show the number of those also detected with the 12 kHz side-scan sonar. The percentage detected within each bin, shown with open circles, is the number detected with the 12 kHz sonar divided by the number found with DSL-120 sonar. Less than one-third of pillow mounds with <60,000 m^2 base area are detected by 12 kHz side-scan, but generally more than half of pillow mounds with larger bases can be resolved. Although not all individual mounds can be identified in the 12 kHz side-scan data, mound fields consisting of many pillow mounds are reliably detected.

Figure 5. Map of the discordant lineaments (black lines) [*Cormier et al.*, 1996] that together with unusually high scarps and bathymetric depth anomalies [*Cormier et al.*, 1996] form the basis for identifying the discordant zones (lighter shaded regions) that are found in OSC migration traces. Definition of discordant lineaments are discussed further in the text. A heavy black line outlines the boundaries of the study area. A thin double line traces the ridge axis through the study area. Arrows point to ends of magmatic segments (L-H) defined by *Sinton et al.* [1991].

Figure 6. Map of the mound fields (dark shaded rectangles) found within the study area, and discordant zones in lighter shading. A heavy black line outlines the boundaries of the study area. A thin double line traces the ridge axis through the study area. The majority of mound fields lie within the discordant zones. Arrows point to ends of magmatic segments (L-H) defined by *Sinton et al.* [1991]. Magmatic segments, the OSC-bounded tectonic segments, and mound fields all coincide.

Figure 7. Sizes of the mound fields, in square kilometers of area covered in map view, compared to the age of the crust near the centroid of the mound field. Crustal age is interpolated as in *Cormier et al.* [1996] from magnetic isochron picks (Doug Wilson, pers. comm., 2000). Error bars represent 0.1 Ma age uncertainty due to the size of the mound fields and the accuracy of the age interpolation. The error bars on the area represent standard error (~3 km^2) . One standard deviation from the mean size encompasses mound fields of 4-80 km^2 area. No statistically significant variation of mound field size with seafloor age is observed within the study area, suggesting that the mound fields are created at or near the EPR axis.

Figure 8. Map of all of the lava fields in the study area that are not associated with off-axis volcanoes. Lava fields are shown as black areas. Off-axis volcanoes are idealized as gray shaded circles scaled to the basal diameter of the volcano [*White et al.*, 1998]. The thick black line marks the boundary of the study area. Slightly thinner black lines are 0.2 Ma and 1 Ma isochrons interpolated as in *Cormier et al*. [1996] from magnetic isochron picks (Doug Wilson, pers comm., 2000). Lava fields are found only close to the ridge axis, on crust less than ~0.2 Ma. The light gray shading shows the axial reflective zone (ARZ) surrounding the ridge axis (shown as thin black double line) picked from 12 kHz sonar data. The ARZ represents a continuous lava field from ridge axis eruptions.

Figure 9. A typical lava field in HMR1 side-scan sonar appears on the right side of the figure as an irregularly shaped darker area dammed against an abyssal hill scarp to the west. Higher backscatter reflectivity is darker shaded. The sonar mosaic was made from three west-looking swaths running northwest. The two different shades of backscatter reflectivity in the lava field may indicate that at least two lava flows comprise this field. The white circles highlight two tiny mounds that might be the source for this field. Very small mounds were found on many of the lava fields in this study, but are not resolved by multibeam bathymetry.

Table 1. Correlation of Mound Fields identified from 12 kHz side-scan sonar to the discordant zones defined by discordant seafloor fabric

	within Discordant Zones	outside Discordant Zones	Total
number of mound fields	76	9	85
area of mound fields	2095 km^2	177 km^2	2272 km^2
% of mound field area	92%	8%	
area of seafloor	16,800 km^2	21,572 km^2	38,372 km^2
mound field area as % of total seafloor	12%	1%	6%

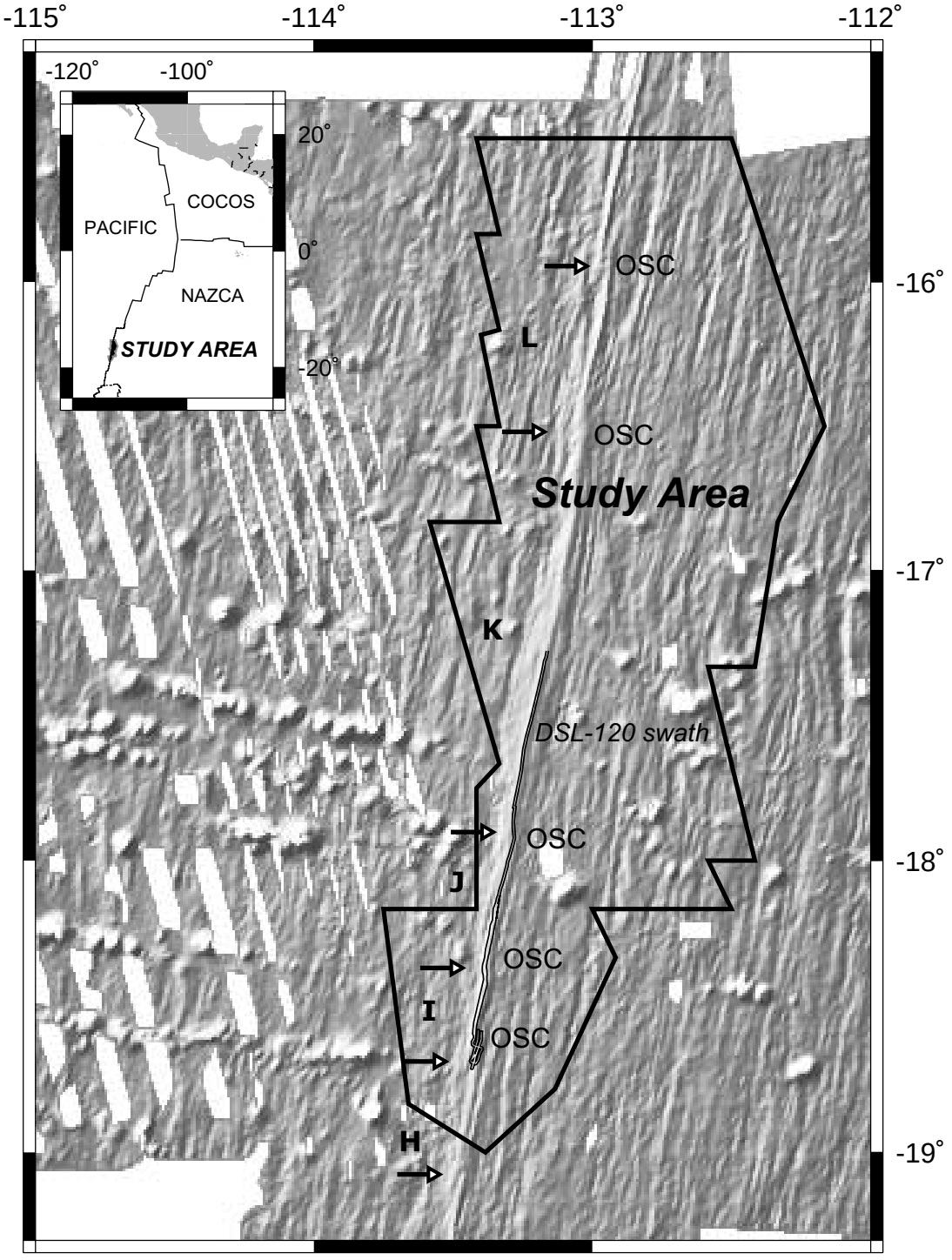
-115˚
-114˚
-113˚
-112˚
-120˚
-100˚
20˚
0˚
-20˚
COCOS
PACIFIC
NAZCA
STUDY AREA
-16˚
-17˚
-18˚
-19˚
OSC
L
OSC
Study Area
K
DSL-120 swath
OSC
J
OSC
I
OSC
H

Figure 1

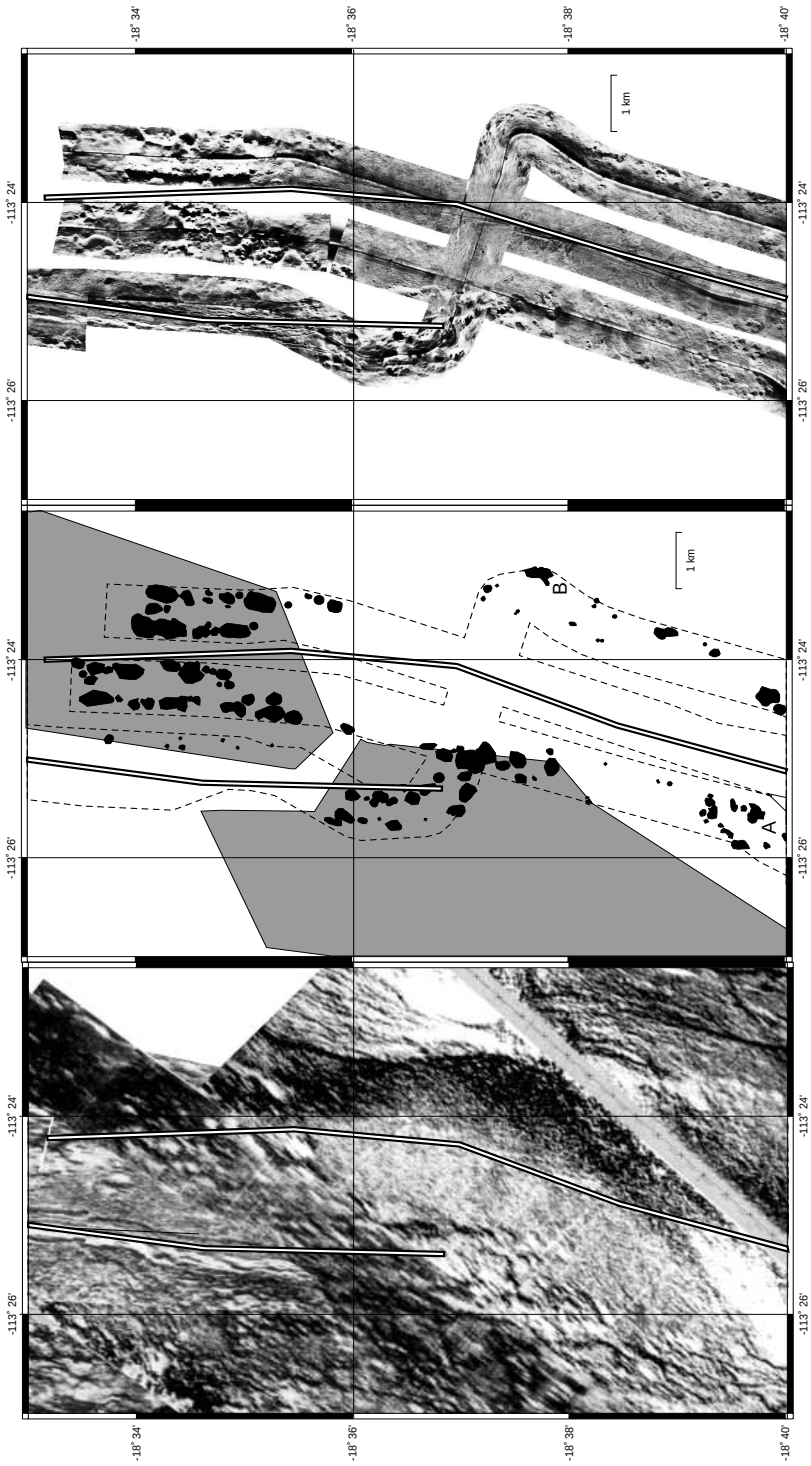

Figure 2

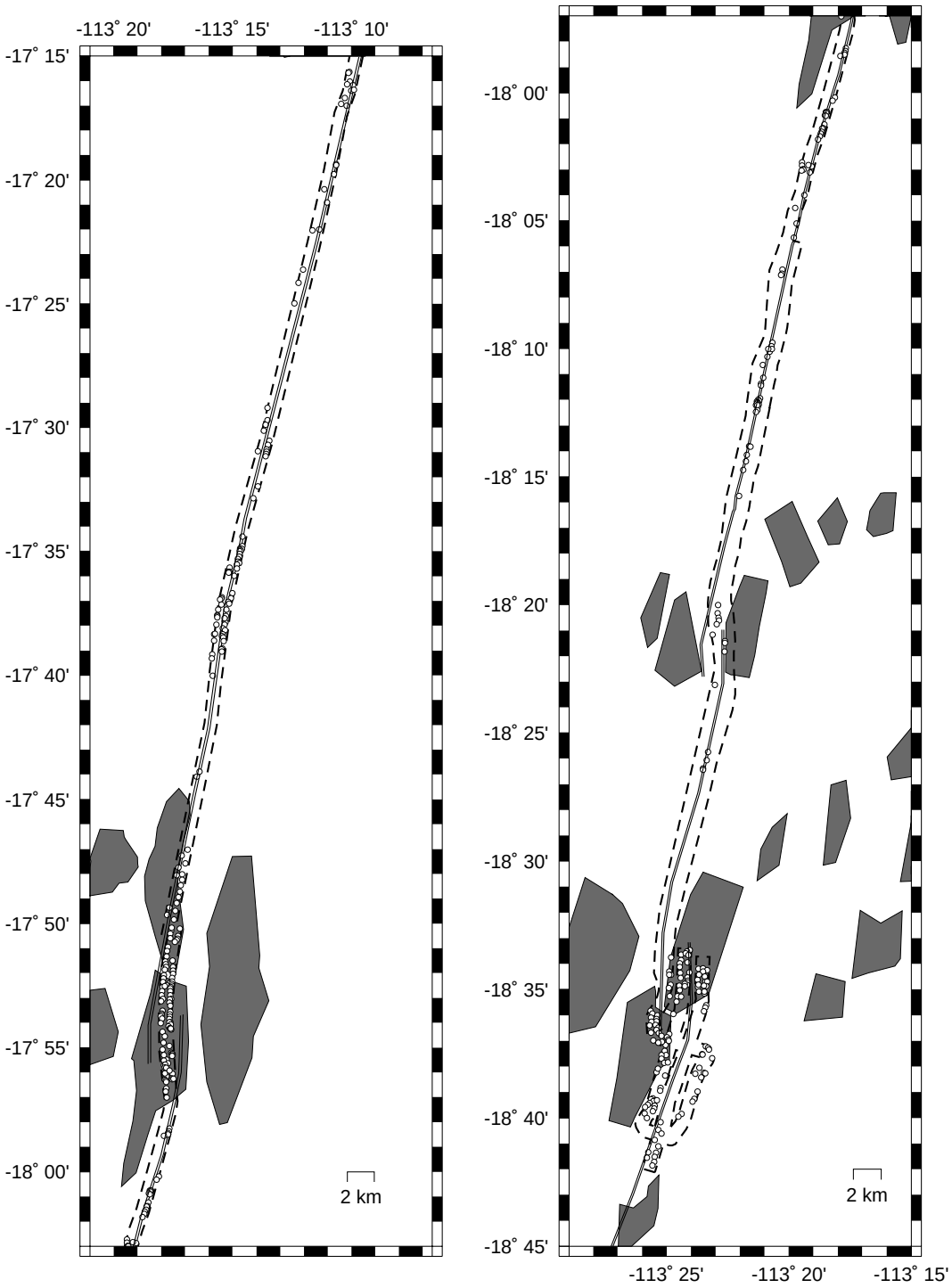
-113° 20'
-113° 15'
-113° 10'
-17° 15'
-17° 20'
-17° 25'
-17° 30'
-17° 35'
-17° 40'
-17° 45'
-17° 50'
-17° 55'
-18° 00'
2 km
-18° 00'
-18° 05'
-18° 10'
-18° 15'
-18° 20'
-18° 25'
-18° 30'
-18° 35'
-18° 40'
-18° 45'
2 km
-113° 25'
-113° 20'
-113° 15'

Figure 3

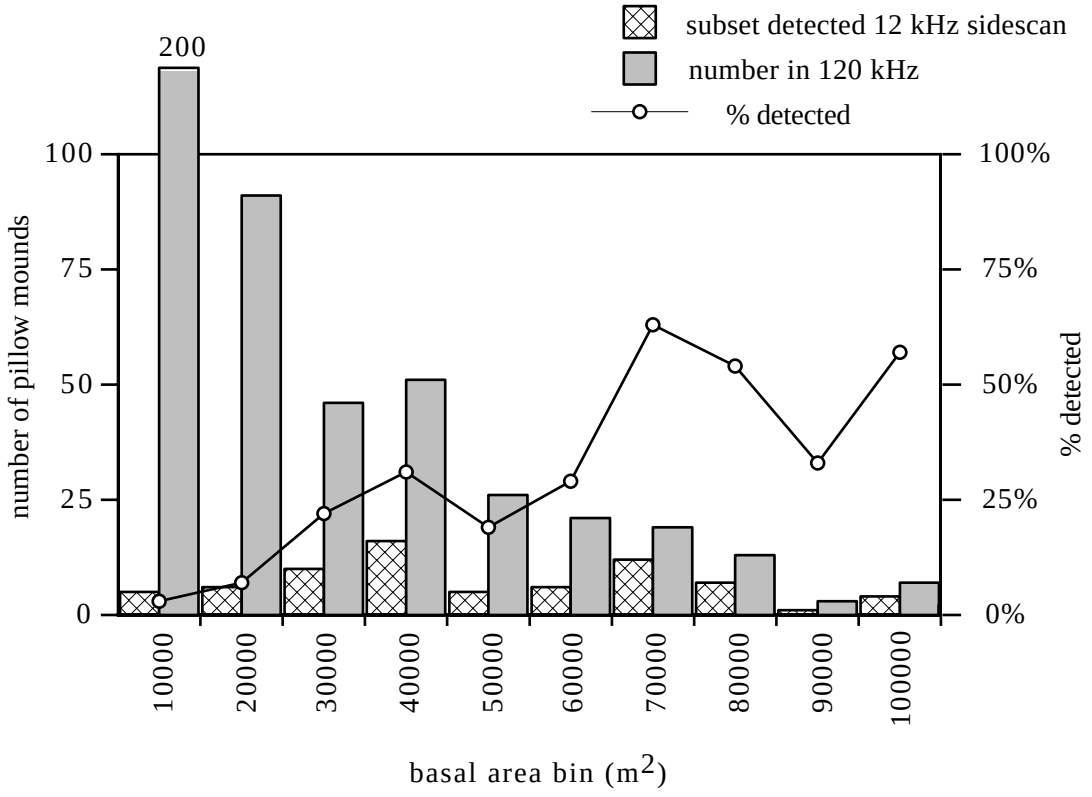
subset detected 12 kHz sidescan
number in 120 kHz
% detected
200
100
75
50
25
0
100%
75%
50%
25%
0%
number of pillow mounds
% detected
10000
20000
30000
40000
50000
60000
70000
80000
90000
100000
basal area bin (m2)

Figure 4

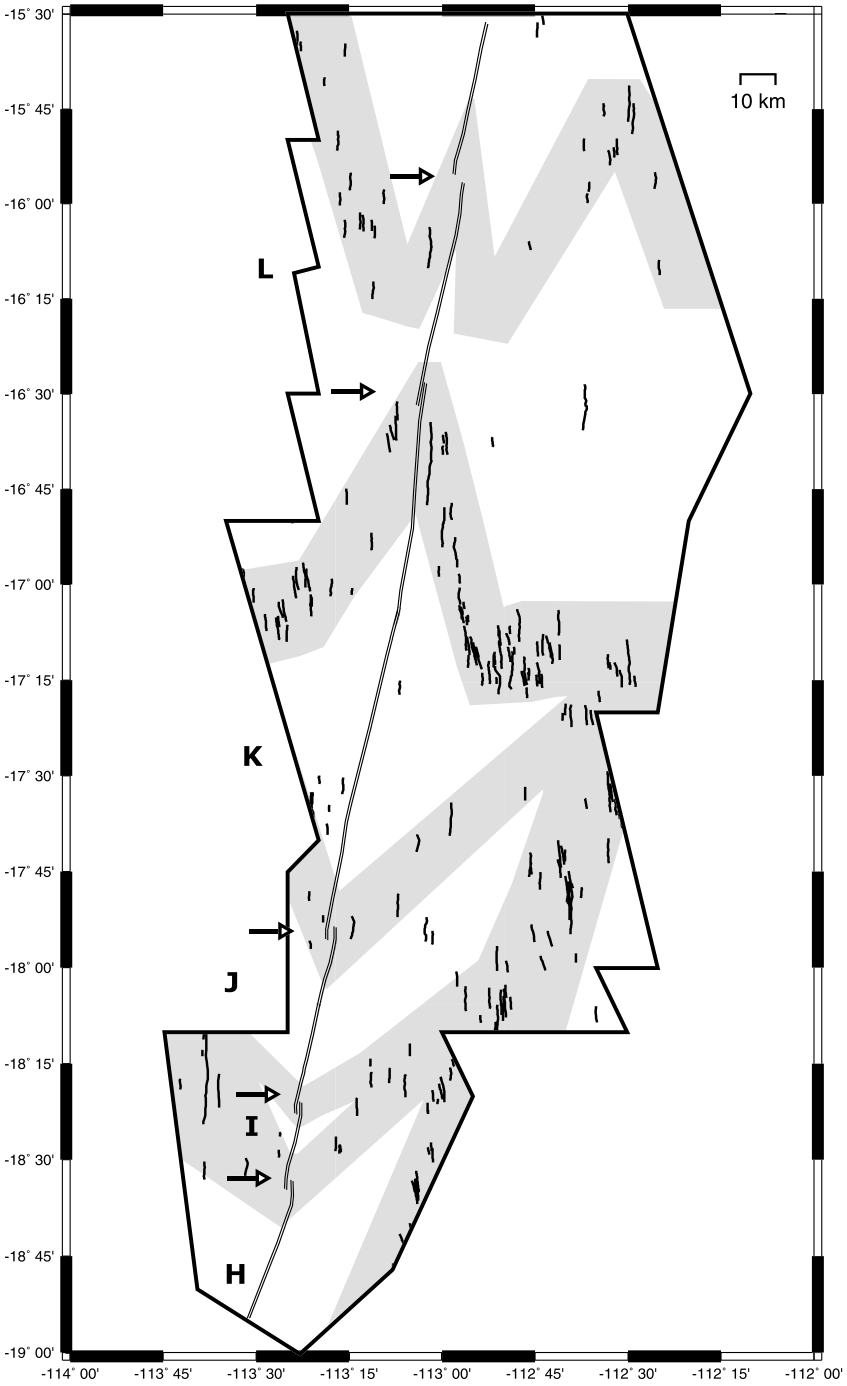
-15° 30'
-15° 45'
-16° 00'
-16° 15'
-16° 30'
-16° 45'
-17° 00'
-17° 15'
-17° 30'
-17° 45'
-18° 00'
-18° 15'
-18° 30'
-18° 45'
-19° 00'
-114° 00'
-113° 45'
-113° 30'
-113° 15'
-113° 00'
-112° 45'
-112° 30'
-112° 15'
-112° 00'
10 km
L
K
J
I
H

Figure 5

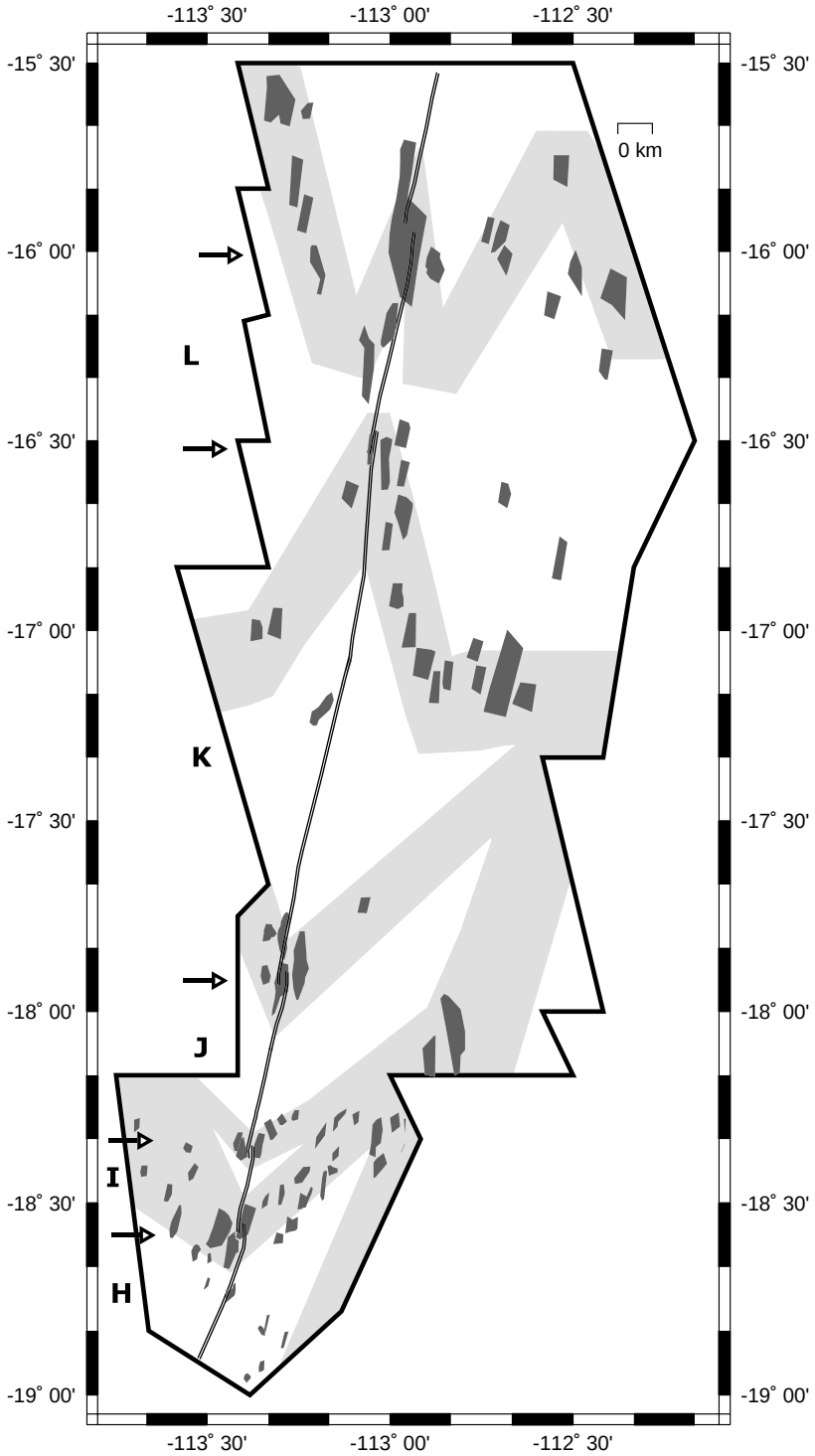
-113° 30'
-113° 00'
-112° 30'
-15° 30'
-16° 00'
-16° 30'
-17° 00'
-17° 30'
-18° 00'
-18° 30'
-19° 00'
0 km
L
K
J
I
H

Figure 6

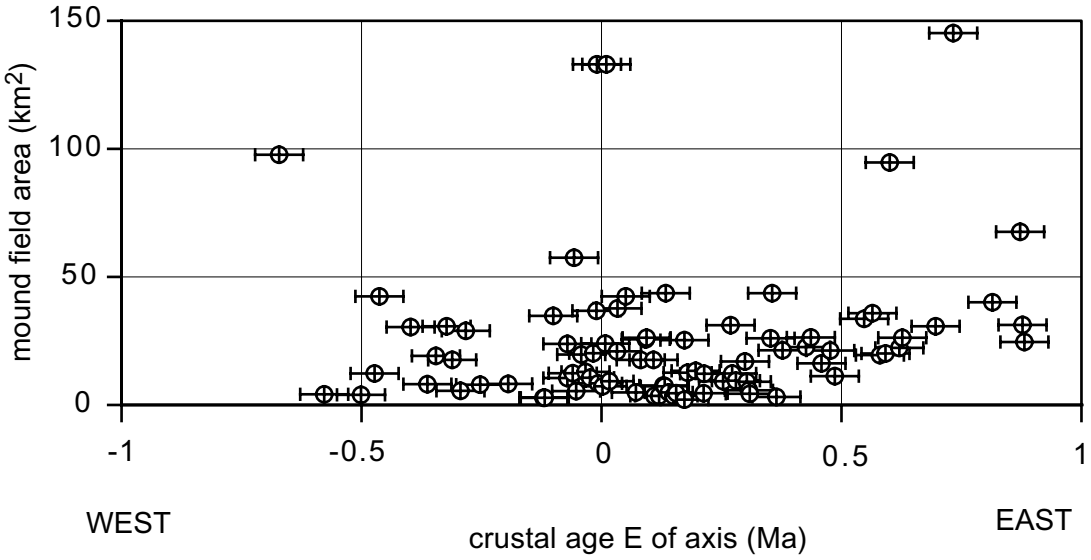
150
100
50
0
mound field area (km2)
-1
-0.5
0
0.5
1
WEST
crustal age E of axis (Ma)
EAST

Figure 7

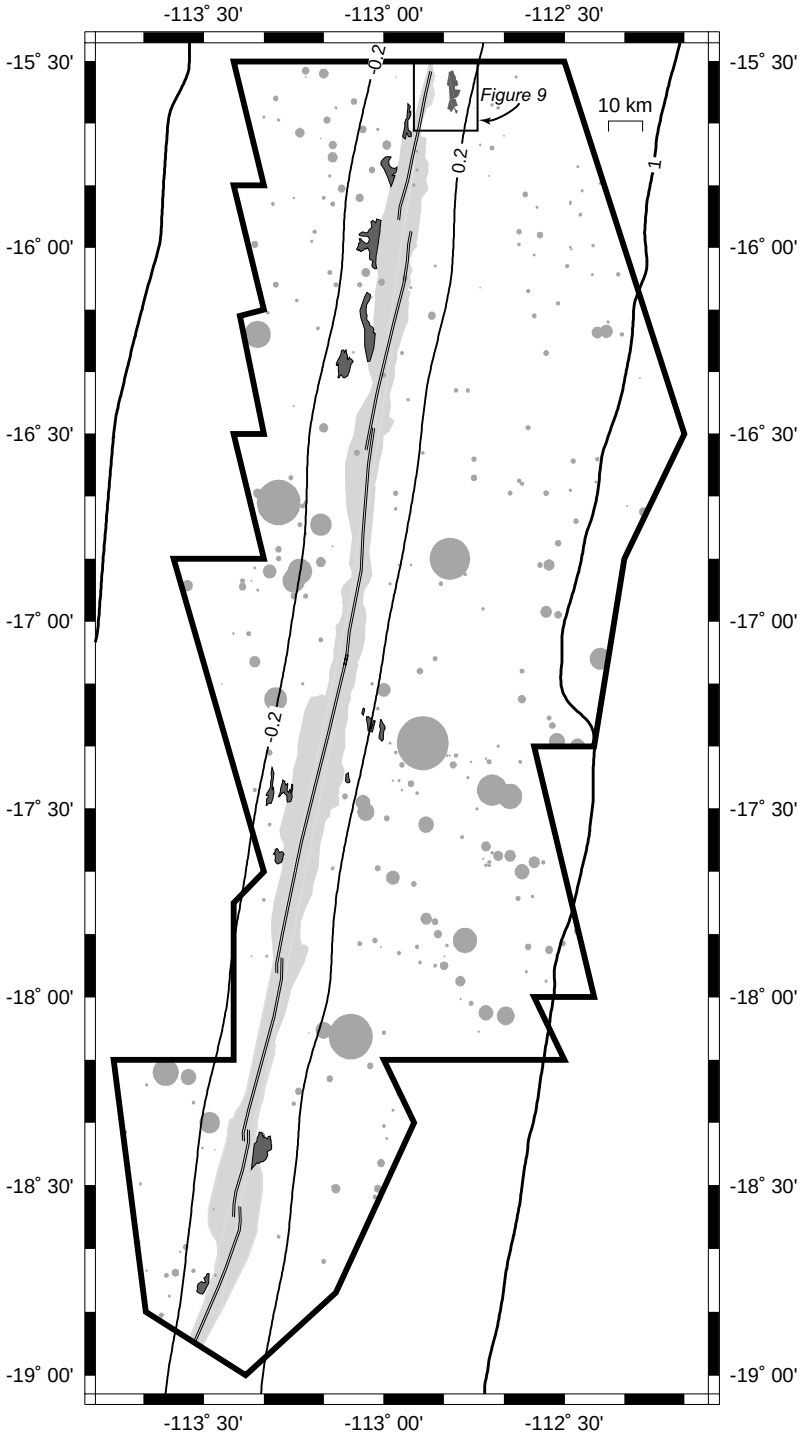
-113° 30'
-113° 00'
-112° 30'
-15° 30'
-16° 00'
-16° 30'
-17° 00'
-17° 30'
-18° 00'
-18° 30'
-19° 00'
-0.2
0.2
1
Figure 9
10 km

Figure 8

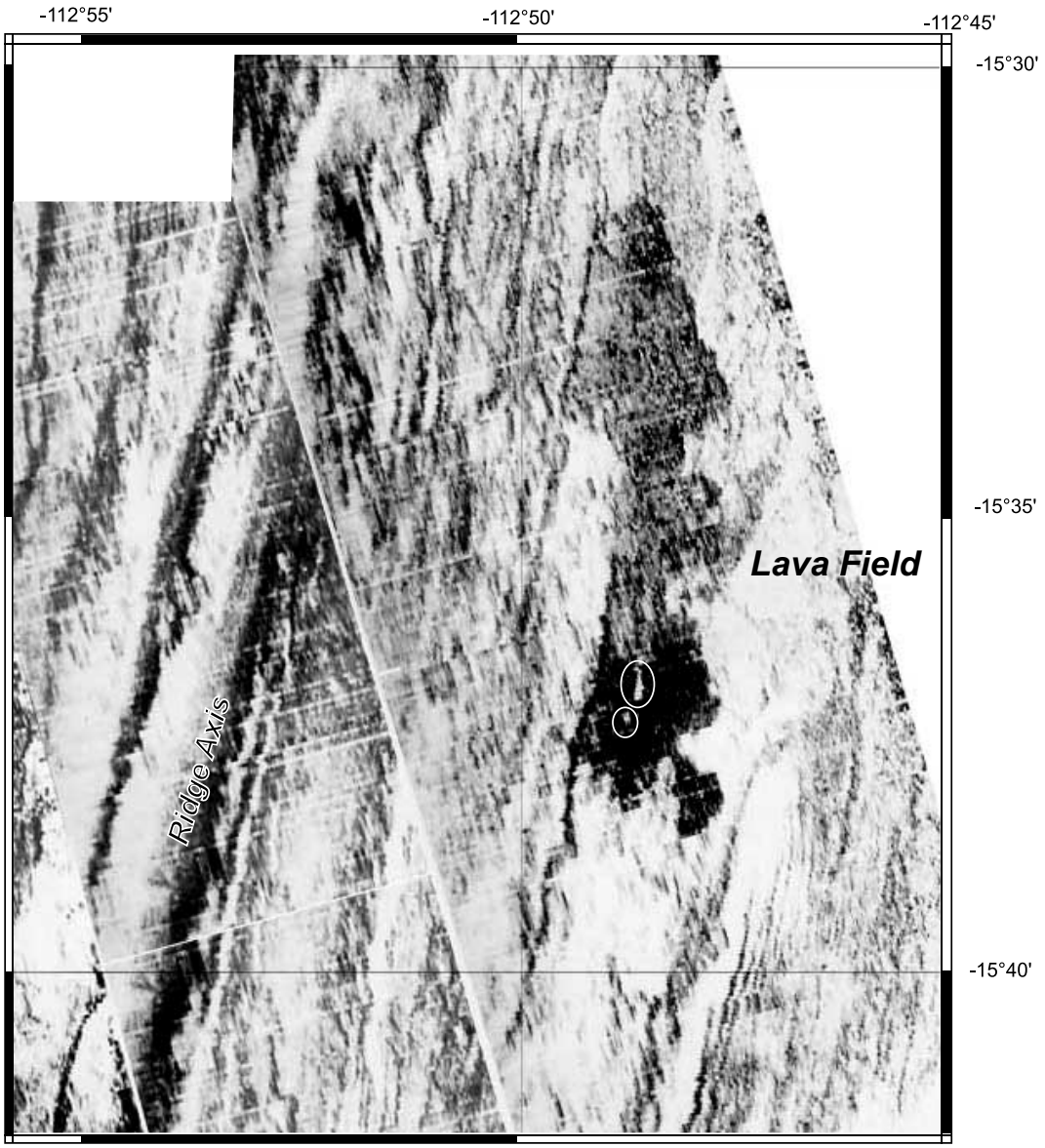

Figure 9